JOURNAL OF AGRICULTURAL AND FOOD CHEMISTRY

Environmental Photochemistry of Tylosin: Efficient, Reversible Photoisomerization to a Less-Active Isomer, Followed by Photolysis

JEFFREY J. WERNER,[†] MAHATI CHINTAPALLI,[‡] RACHEL A. LUNDEEN,[§] KRISTINE H. WAMMER,[§] WILLIAM A. ARNOLD,*[,†,‡] AND KRISTOPHER MCNEILL*[,†,#]

Water Resources Science Program, University of Minnesota, 1985 Buford Avenue, St. Paul, Minnesota 55108, Department of Civil Engineering, University of Minnesota, 500 Pillsbury Drive SE, Minneapolis, Minnesota 55455, Department of Chemistry, University of Saint Thomas, 2115 Summit Avenue, St. Paul, Minnesota 55105, and Department of Chemistry, University of Minnesota, 207 Pleasant Street SE, Minneapolis, Minnesota 55455

The environmental photochemical kinetics of tylosin, a common veterinary macrolide antibiotic and growth promoter, were investigated under simulated sunlight. An efficient, reversible photoisomerization was characterized using kinetic, mass spectrometry, and proton nuclear magnetic resonance data. The photoisomerization was confirmed to occur by a rotation about the distal alkene of the ketodiene functionality. Concurrent forward (quantum yield $= 0.39 \pm 0.09$) and back (quantum yield $= 0.32 \pm 0.08$) reactions lead to a photochemical equilibrium near a tylosin/photoisomer ratio of 50:50, completed in less than 2 min under a spectrum equivalent to noontime, summer sunlight. The activity of the isomer for the inhibition of *Escherichia coli* DH5α growth was observed to be less than that of tylosin. On a longer time scale than that of isomerization, the isomer mixture undergoes photolysis with a quantum yield of $(1.4 \pm 0.3) \times 10^{-3}$. The observed quantum yields and UV−vis absorbance data allow for the prediction of the photochemical behavior of tylosin in most environmental systems. Indirect photosensitization was not a significant loss process in solutions of Suwannee River fulvic acid with concentrations from 1 to 20 mg L^{-1}.

KEYWORDS: Tylosin; environmental fate; photolysis; quantum yield; antibiotic activity

INTRODUCTION

Tylosin, a widely used veterinary antibiotic in the U.S., is often included daily in poultry and swine feed as a growth promoter. Its use is associated with a sharp increase in the prevalence of genes for macrolide resistance, including resistance to erythromycin, an important macrolide antibiotic in human medicine (*1*). There is concern that a pathway may exist from the administration of tylosin as a growth promoter to the occurrence of macrolide resistance in human pathogens. Aside from the direct interaction of people and livestock, one important pathway might be initiated by the spreading of animal waste on agricultural fields. The concurrent application of unmetabolized tylosin and resistant intestinal bacteria to an environmental system may offer a mechanism for the development or proliferation of resistance genes. A recent study by Onan and LaPara showed evidence for this mechanism in fields where manure was spread (*2*). Additionally, tylosin has been detected in surface waters in numerous locations throughout the U.S. (*3*).

The environmental fate of tylosin is an important component in the assessment of the risk posed by application of tylosin-containing manure to fields. Tylosin stability has been observed in field studies to have a half-life of 40−86 days (*4*), with loss processes including biodegradation ($t_{1/2} = 2-40$ days; *5*, *6*) and hydrolysis ($t_{1/2} \approx 9.6$ days, $6 < \text{pH} < 8$; *7*), both of which are limited by the availability of the compound in the aqueous phase ($\log K_d \approx 2$; *8*). In laboratory microcosms, tylosin degrades to a number of products including tylosin B, tylosin C, and tylosin D (the parent compound, tylosin A, is referred to herein as "tylosin") and also forms a photoisomer (*9*−*11*). Halling-Sørensen et al. (*9*) have observed that the rapid formation of these products leads to a significant reduction in potency. Hu and Coats (*11*) recently observed tylosin loss in water to have a half-life of 200 days verses a much shorter half-life in soil of 7 days. Although Hu and Coats (*11*) noted that the experimental conditions filtered out a majority of the UVA and UVB wavelengths which tylosin absorbs, they observed two photo-

* To whom correspondence should be addressed. E-mail: arnol032@umn.edu. Phone: 612-625-8582 (W. A. Arnold). E-mail: mcneill@chem.umn.edu. Phone: 612-625-0781 (K. McNeill).
[†] Water Resources Science Program, University of Minnesota.
[‡] Department of Civil Engineering, University of Minnesota.
[§] Department of Chemistry, University of St. Thomas.
[#] Department of Chemistry, University of Minnesota.

10.1021/jf070101h CCC: $37.00
Published on Web 07/26/2007

isomerization products at low concentrations. One of these products they suggested to be an photoisomer previously observed by Paesen et al. (*10*), which was proposed to result from rotation about the distal alkene on the ketodiene functionality. Tylosin is known to be unstable upon exposure to sunlight. The previous studies cited here begin to suggest photochemical pathways, but there have been no studies to date of the photolysis kinetics of tylosin under a solar spectrum. If transport and degradation in surface waters is to be considered as an important component of the environmental fate of tylosin, knowledge of its photochemical behavior will be helpful.

In this study, the aqueous photochemical kinetics of tylosin were investigated under simulated sunlight. A fast photochemical equilibrium was observed and attributed to a reversible photoisomerization. The rapid process is followed by the slower, simultaneous photolysis of the two photoisomers. The antibiotic activity of the photoisomer was also quantified and was found to be less than that of tylosin.

MATERIALS AND METHODS

Materials. Tylosin A tartrate salt (95%, absence of tylosin B, tylosin C, and tylosin D verified by HPLC/UV−vis and MS, described below), *p*-nitroanisol (PNA; 98%), and pyridine (PYR; 99+%) were used as supplied from Sigma-Aldrich (Milwaukee, WI). Iso-Sensitest bacterial (ISB) growth medium was purchased from Oxoid (Ogdensburg, NY). All aqueous solutions were made fresh daily in Milli-Q ultrapure water (Millipore Corporation, Billerica, MA). Suwanee River fulvic acid (SRFA) was obtained from the International Humic Substances Society (St. Paul, MN).

Photolysis. Photolysis was carried out in a Suntest CPS+ solar simulator with a UV-Suprax optical filter (Atlas Materials Testing Solutions, Chicago, IL). Solutions were irradiated in quartz test tubes (o.d. = 1.3 cm, i.d. = 1.1 cm, $V = 10$ mL) positioned to face the lamp perpendicularly. Light intensity was monitored using the *p*-nitroanisol/pyridine (PNA/PYR) actinometer method of Dulin and Mill (*12*).

Photochemical kinetics were monitored via subsamples taken at regular time intervals and later quantified by high-pressure liquid chromatography (HPLC) with UV−vis detection as described below. Selected photolysis time points were also analyzed by UV−vis absorbance using a Shimadzu UV-1601 PC spectrophotometer (Kyoto, Japan). Photolysis kinetics were monitored over both a long, 2 h, time period as well as a short, 4 min, time period to capture the two distinct portions of the kinetic time series that were observed. Photolysis was repeated for solutions of both 10 μM and 100 μM tylosin and at both pH 4.3 and 9.1. Solar quantum yields were calculated as described in Zepp (*13*; see Supporting Information for details).

Additional photolysis experiments were performed in various concentrations of Suwanee River fulvic acid (SRFA) to test for any significant indirect sensitization effects. Solutions of 1, 5, 10, and 20 mg L^{-1} SRFA and 100 μM tylosin were adjusted to a pH of 8.0 and irradiated as described above. The UV−vis absorbance spectra of these solutions were measured and used to correct for light screening as described in the Supporting Information, based on Leifer (*14*) and Schwarzenbach et al. (*15*).

Instrumental Analysis. Tylosin concentrations were quantified with a Hewlett-Packard series 1100 HPLC (Santa Clara, CA) using a Supelco (Milwaukee, WI) C16 RP-Amide 150 mm × 4.6 mm, 5 μm particle size column with an in-line RP-Amide C16 guard column, a flow rate of 1 mL min^{-1}, an acetonitrile/pH 3 phosphate buffer gradient from 10:90 (0 min) to 46:54 (4 min) and held for 4 min. Detection was performed using UV−vis absorption at 290 nm.

^{1}H NMR analysis was performed on $CDCl_3$ and D_2O solutions of 1.0 mM tylosin, both before and after 4 min of photolysis. ^{1}H NMR spectra were obtained with a 500 MHz Varian Inova with a 5 mm H{P−X} triple resonance, *Z*-axis PFG probe. Solutions prepared for ^{1}H NMR analysis were also analyzed by HPLC, as described above, to verify the extent of isomerization.

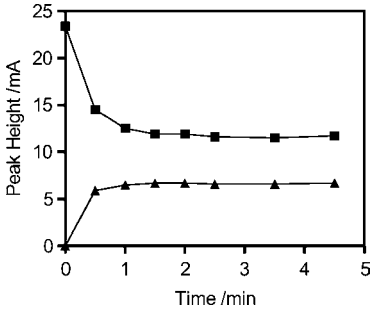

Figure 1. The loss of the tylosin peak (■) as monitored by HPLC/UV–vis and the growth of the product peak at a retention time of 6.5 min (▲).

Mass spectrometry was performed on an aqueous 100 μM tylosin solution both before and after 2 min of photolysis. Spectra were obtained using a Bruker BioTOF II time-of-flight (TOF) mass spectrometer (MS) with positive ion electrospray ionization (ESI). The *m*/*z* range 101−1009 was acquired for samples before and after photolysis, as well as those performed with a PPG (poly(propylene glycol)-716) high-resolution *m*/*z* internal standard. An additional spectrum with the *m*/*z* range 101−2012 was taken of the postphotolysis sample to verify that no higher molecular weight compounds were formed. Solutions prepared for MS analysis were also analyzed by HPLC, as described above, to verify the extent of isomerization.

Antibiotic Activity Assay. The antibiotic activities of tylosin and the proposed isomer for the inhibition of *Escherichia coli* DH5α growth were determined by the method described in Wammer et al. (*16*). A fresh solution of 9 mM aqueous tylosin was divided into two fractions, one irradiated to isomerization equilibrium and the other stored in the dark. The extent of photoisomerization was measured by HPLC/UV−vis. Equal aliquots of the pre- and postirradiation solutions were added to parallel test tubes containing 9 mL of sterile ISB, which was made by adding 23.4 g of ISB powder per liter of pH 7 phosphate buffer (4.9 g of KH_2PO_4 and 9.7 g of Na_2PO_4 per liter deionized water). This was done for a series of test tube sets to achieve total tylosin (or tylosin plus isomer) equivalent concentrations of 990, 495, 297, 198, 149, 99, 50, 9.9, and 0 μM. Additional water was added to each tube, accordingly, to make the volumes equivalent. To initiate the 8 h growth period, 100 μL aliquots of *E. coli* DH5α liquid culture grown overnight on ISB were added to each tube. Tubes were incubated at 37 °C, shaking at 200 rpm. Each treatment was performed in triplicate. After 8 h of growth, the optical density was measured as absorbance units (AU) at 600 nm (OD_{600}).

The data were fit to the Boltzmann curve in eq 1, where x is the log

$$y = A_2 + \frac{(A_1 - A_2)}{1 + \exp[(x - x_0)/dx]} \quad (1)$$

of tylosin concentration, x_0 is the midpoint of the curve (the effective concentration for 50% inhibition, EC_{50}), dx is the slope factor of the curve, y is the change in OD_{600} over 8 h, A_1 is the value of y at the top of the curve, and A_2 is the value of y at the bottom of the curve. The initial OD_{600} of each vial and any change in OD_{600} for noninoculated control solutions were subtracted from the data before curve-fitting.

RESULTS

Kinetics. The photolysis of tylosin was observed to occur in two major steps: formation of a rapid photochemical equilibrium, followed by photochemical loss on a slower time scale. HPLC/UV−vis data illustrating the initial, rapid step are shown in **Figure 1**. Tylosin equilibrates to approximately one-half of its original concentration, accompanied by the formation of a product peak of a slightly greater retention time (sample chromatograms included in Supporting Information). The equilibrium between tylosin and the product peak was observed to be stable at room temperature in the dark for over 48 h.

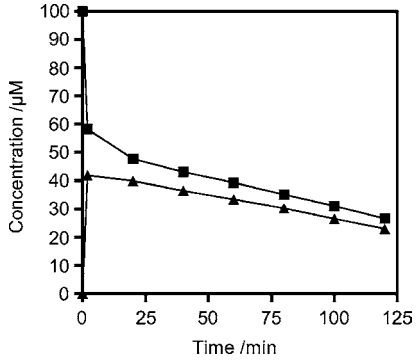

Figure 2. Photolysis time series showing tylosin concentration (■) and the observed product (▲), highlighting the longer time scale degradation process. Concentration of product calculated assuming 1:1 transformation of tylosin to product in the equilibrium shown in **Figure 1**.

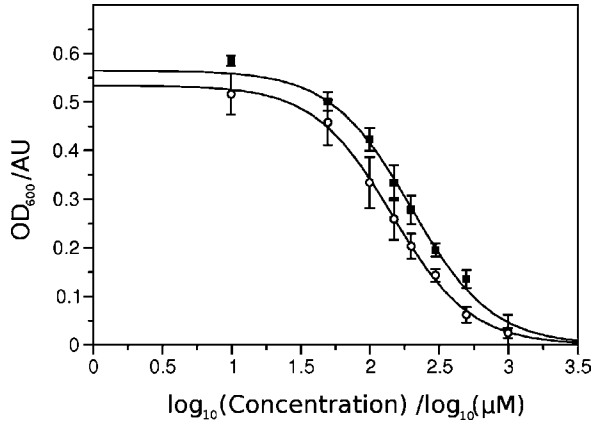

Figure 3. The OD_{600} after 8 h *E. coli* growth in culture tubes containing various concentrations of tylosin. Data shown are for the control tylosin solution (○) and the same solution following photoisomerization (■). Concentration is plotted as the sum of tylosin and isomer and thus is normalized to the volume of stock solution used. Error bars represent the standard deviation of triplicate experiments.

The photochemical equilibrium was independent of concentration and pH. For 10 and 100 μM initial tylosin concentrations, the relative tylosin concentration at equilibrium was the same in both cases, at approximately one-half of its initial value. See Supporting Information for kinetic data. The solutions at both pH 4.3 and 9.1 (tylosin $pK_a = 7.1$) showed identical UV−vis absorbance spectra and photolysis kinetics (see Supporting Information).

Tylosin and the observed product peak later identified as a photoisomer underwent a simultaneous loss process on a longer time scale following the fast step observed in **Figure 1**. The concentrations of tylosin and the photoisomer as a function of time over 120 min of irradiation are shown in **Figure 2**. The concentration of the isomer was calibrated using the relative instrument response in **Figure 1**, assuming a 1:1 transformation of tylosin to the isomer. The pseudo-first-order rate constant for the longer time scale loss process ($t > 2$ min) in **Figure 2** was $(9.9 \pm 0.6) \times 10^{-5}$ s^{-1}, where the error reported is the standard error of linear regression of the ln(concentration) versus time data.

Photolysis in the presence of varied concentrations of SRFA showed no sensitization effect. A slight decrease in the pseudo-first-order rate constant was observed with the addition of SRFA. This decrease in rate constant was attributable to the light-screening effect of the added SRFA. Photolysis rate constants are plotted as a function of [SRFA] in the Supporting Information, alongside the theoretical rate constants expected for direct photolysis considering the light screening effect.

Table 1. Assignment of ^{1}H NMR Chemical Shifts (ppm) and Coupling Constants (Hz) for Each of the Protons in the Ketodiene Chromophore of Tylosin, along with Assignment of the Analogous Protons of the Product of the Rapid Photochemical Equilibrium

position of proton relative to the ketone	chemical shift in ppm (*J* in parentheses in Hz)	
	tylosin	product isomer
α	6.29 (15)	6.23 (15)
β	7.33 (15)	7.65 (15)
δ	5.92 (10)	6.01 (10)

Proton NMR. The vinyl region of the tylosin ^{1}H NMR spectrum in $CDCl_3$ was compared before and after the equilibrium in **Figure 1** was reached (4 min of photolysis). Chemical shifts were assigned based on the complete ^{1}H NMR assignment available in the study by Simova and Ivanova (*17*). Protons with a chemical shift upfield of 5.5 ppm were not resolved in the current study. The protons in the ketodiene chromophore of tylosin, however, were well resolved and can be seen in the Supporting Information. Protons were assigned to peaks as listed in **Table 1**, including chemical shifts and coupling constants. Establishment of the photochemical equilibrium pictured in **Figure 1** was confirmed by HPLC analysis. Spectra in D_2O agreed with those taken in $CDCl_3$, except for the additional splitting of peaks in D_2O due to epimerization of the chiral center adjacent to the ketone via tautomerization and proton (or deuterium) exchange with the solvent (*17*).

Mass Spectrometry. Mass spectra both before and after photolysis are shown in the Supporting Information. There was no observed change, including no new *m*/*z* peaks detected after the photochemical equilibrium was reached. The major peak at $m/z = 916$ corresponds to the mass of [tylosin$-H^+$], with a measured high-resolution *m*/*z* value of 916.5280 ± 0.0012 (theoretical monoisotopic exact mass of 916.5264, error = 1.7 ppm, $n = 3$). Establishment of the photochemical equilibrium pictured in **Figure 1** was confirmed by HPLC analysis.

Antibiotic Activity Assay. Figure 3 shows the OD_{600}, 8 h after inoculation, of the *E. coli* DH5α cultures as a function of tylosin concentration. Overlaid is a parallel experiment in which the tylosin stock solution had been irradiated to photoisomerization equilibrium (verified by HPLC analysis). The data in **Figure 3** were fit to eq 1 using the nonlinear least-squares Marquardt−Levenberg algorithm as implemented in gnuplot 4.0. The fit included consideration of the scatter of replicates, as well as the OD_{600}(8 h) of the control vials (data not plotted; OD_{600}([tylosin] = 0) = 0.54 ± 0.04 AU). The curves which resulted from the fits are shown as solid lines in **Figure 3**. For the control tylosin solution, fitting yielded $x_0 = EC_{50} = 2.16 \pm 0.04$ log(μM), d$x = 0.29 \pm 0.04$ log(M), $A_1 = 0.53 \pm 0.01$ AU, and $A_2 = 0.00 \pm 0.03$ AU. For the postirradiation tylosin/isomer mixture, fitting yielded $x_0 = EC_{50} = 2.31 \pm 0.04$ log(μM), d$x = 0.30 \pm 0.04$ log(M), $A_1 = 0.56 \pm 0.01$ AU, and $A_2 = -0.01 \pm 0.04$ AU. The errors are the asymptotic standard errors reported as output from gnuplot. The noninoculated control solutions showed no growth. After irradiation of the 9 mM tylosin solution, the tylosin/isomer ratio was observed to be 63:37 (higher than other experiments performed at lower concentrations, attributable to light screening and incomplete photoisomerization).

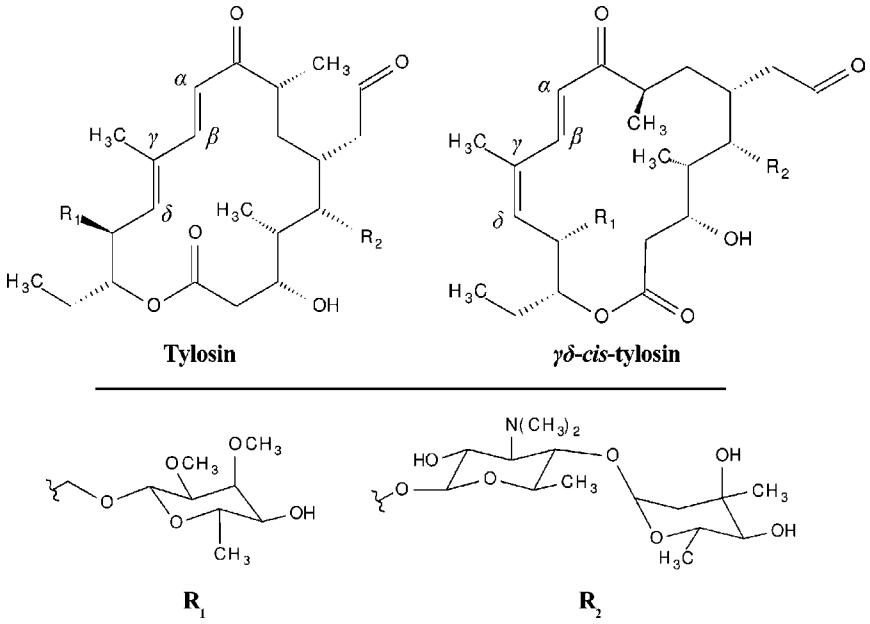

Figure 4. Structures of tylosin and the proposed product isomer, γ/δ-*cis*-tylosin.

DISCUSSION

Photoisomerization. The rapid equilibration process shown in **Figure 1** was concluded to be a reversible photoisomerization. The isomerization is proposed to be a rotation about the γ/δ double bond of the ketodiene chromophore of the tylosin macrolide ring, as was previously observed by Paesen et al. (*10*). The structure of tylosin as well as that of the proposed isomer are shown in **Figure 4**. There are several kinetic lines of evidence supporting the proposed isomer. The lack of concentration dependence in the kinetic data rules out any bimolecular reaction as the rate-limiting step. A bimolecular reaction leading to a photochemically driven equilibrium between tylosin and the product would lead to different equilibrium values at different initial tylosin concentrations. The same would be true for a reaction of excited-state tylosin with a second tylosin molecule or any mechanism for the limited, irreversible transformation of tylosin to the product (including reactions which involve a second limiting reactant). The kinetic evidence indicates a photochemically driven unimolecular equilibrium as the rate-limiting step. A similar kinetic scheme has been observed for the environmental photochemistry of some nitrofuran antibiotics (*18*). The MS data also indicate that the product is an isomer of tylosin, as no additional *m*/*z* peaks were observed following photolysis.

The photoisomerization shows no dependence on protonation state of tylosin or on the solvent used. This rules out solvent-catalyzed rearrangements or any intramolecular electron transfer or proton-transfer mechanisms involving the dimethyl amine moiety in R_2 (the site of protonation). The most likely scenario is rotation about one of the double bonds of the chromophore. The ^{1}H NMR coupling constant for the vinyl protons located α and β to the ketone was observed to remain that of trans coupling, with $J = 15$ Hz, eliminating the possibility of rotation about the α/β double bond. This is in agreement with the ^{1}H NMR observations in Paesen et al. (*10*) and leaves rotation about the γ/δ double bond as the most likely photoisomerization process. Hu and Coats (*11*) observed two different isomers as products during tylosin loss associated with light exposure in environmental microcosms. One isomer appeared quickly and they proposed it to be the γ/δ-*cis*-tylosin isomer identified by Paesen et al. (*10*) and characterized in this study. Appearance of a second, unidentified isomer, occurred after a significant time delay (*11*). Under the conditions and time scale of our current photolysis experiments, no second isomer was observed. The lack of additional observed isomers in the current study could result from inadequate chromatographic resolution, though this seems unlikely because the ^{1}H NMR data indicate that there is only one significant photoisomerization which affects the vinyl protons of the ketodiene functionality.

Kinetics. The photochemical equilibrium in **Figure 1** is established on a time scale which is much shorter than the subsequent degradation. This conveniently results in the initial step being completely deconvoluted from the second. The rate constants for the rapid photoisomerization were therefore able to be calculated assuming the simple kinetics of the reaction in eq 2.

$$\text{tylosin} \underset{k_{\text{iso},-1}}{\overset{k_{\text{iso},1}}{\rightleftharpoons}} \text{isomer} \tag{2}$$

The only processes which were considered to model the data in **Figure 1** were the photochemical transformation of tylosin to the isomer by the pseudo-first-order rate constant $k_{\text{iso},1}$, and the pseudo-first-order photochemical transformation of the isomer back to tylosin by the rate constant $k_{\text{iso},-1}$. The concentration of tylosin at time t, C_t, relative to the initial concentration C_0 was calculated using the assumption of a 1:1 yield for transformations between tylosin and the isomer (i.e., [isomer] $= C_0 - C_t$), resulting in eq 3.

$$\frac{C_t}{C_0} = \left(\frac{k_{\text{iso},1}}{k_{\text{iso},1} + k_{\text{iso},-1}}\right) \exp[-(k_{\text{iso},1} + k_{\text{iso},-1})t] + \frac{k_{\text{iso},-1}}{k_{\text{iso},1} + k_{\text{iso},-1}} \tag{3}$$

This equation was fitted to the data to give the rate constants $k_{\text{iso},-1} \approx k_{\text{iso},1} = (2.8 \pm 0.6) \times 10^{-2}\ \text{s}^{-1}$ (error represents standard error for the fit to the data). There was no significant difference between the backward and forward rate constants because the equilibrium tylosin concentration was one-half its initial value ($C_t/C_0 = 0.50 \pm 0.01$, where the error reported represents the standard deviation of the concentration data after equilibrium: $t \geq 1.5$ min). A figure showing the concentration-corrected data

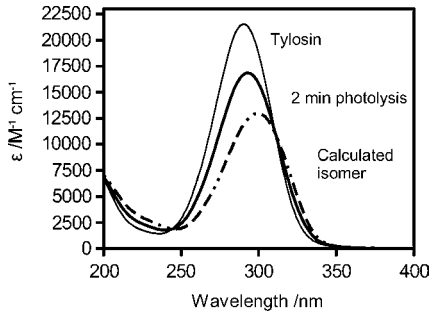

Figure 5. UV–vis absorptivity (ϵ) of aqueous tylosin before and after 2 min of irradiation and the calculated absorptivity spectrum of the isomerization product.

fit to eq 3 is available in the Supporting Information. Because of the magnitude of the difference between the kinetics of the fast step and the slow step, the deconvolution of kinetic parameters for this system was much simpler than the similar kinetic system observed in Edhlund et al. (*18*).

The presence of SRFA affected neither the photoisomerization equilibrium nor the subsequent photochemical loss. This is in agreement with the observation that the direct photolysis routes for both processes are rapid. It was also concluded from preliminary UV−vis absorbance spectra (data not shown) that the presence of 0.1 M calcium cations had no effect on the chromophore, and presumably no significant chelation was occurring. Prediction of photochemical loss of tylosin is simplified by the lack of dependence on a number of variables, including pH, sensitizers, and water hardness. The longer degradation process, after correcting for the $\times 2$ lens effect of the test tubes, corresponds to approximately 3.9 h half-life at the water surface, at noon, in the summer, in Minneapolis, MN.

Quantum Yield Values. The photoisomerization of tylosin to γ/δ-*cis*-tylosin was calculated to have a quantum yield of 0.39 ± 0.09. All quantum yields reported were calculated for the average light spectrum of the solar simulator, according to the method described in Zepp (*13*). The error for all reported quantum yield values was propagated from the error in the respective pseudo-first-order rate constant. Calculation of the quantum yield for the back reaction from the isomer to tylosin requires an estimate of the molar absorptivity spectrum of the isomer. This spectrum was calculated from the absorbance of the tylosin/isomer 50:50 mixture, subtracting the known absorbance of tylosin. The resultant spectra, normalized to molarity and path length, are shown in **Figure 5** and tabulated in the Supporting Information. The isomer peak is shifted to slightly longer wavelengths and is lowered in intensity. The total photochemical action of the isomer in the solar simulator is 20% greater than that of tylosin, due to the absorbance shift to longer wavelengths where the lamp intensity is greater. The quantum yield of the isomerization from γ/δ-*cis*-tylosin to tylosin was calculated to be 0.32 ± 0.08.

The high quantum yield values, near one-half, for both the forward and back reactions indicate that, within the photochemical action of the system, a large fraction (near unity) of the photon absorption events lead to a triplet excited-state with free rotation about the γ/δ double bond. The tylosin macrolide ring structure is flexible, with a number of favorable conformations (*19*). This partially explains the little or no observed preference for either the cis or trans conformation of the γ/δ double bond when returning to the ground state. We propose that all of the photochemical processes observed here (isomerization and degradation) of both tylosin and its photoisomer take place from a common triplet excited-state intermediate.

The slower photolysis step proceeds with a quantum yield of $(1.4 \pm 0.3) \times 10^{-3}$. It is not possible to calculate the individual quantum yields of either pure tylosin or the isomer. Because the photochemical equilibration takes place more quickly than the photolysis, the only observable loss in the rate constant is that of the average loss of the sum of tylosin and the isomer. If, as expected, excitation of both compounds leads to the same triplet excited state, the photolysis quantum yield should be equal for tylosin and the isomer.

Antibiotic Activity. Upon inspection of **Figure 3**, it can be seen that the photoisomer γ/δ-*cis*-tylosin has an antibiotic activity lower than that of tylosin. The post-photolysis concentration values (*x*-axis) are plotted as the concentration of tylosin in the pre-photolysis solution, or (equivalently) the sum of tylosin and isomer concentrations. This value was chosen as the independent variable for several reasons: (1) The alignment of data along the *x*-axis is consequently normalized to the total volume of stock solution added; thus, any observed shift in the curve position cannot be attributed to the systematic effect of a contaminant in the stock solution (if one were present). (2) The statistical significance of a reported difference in activity can be visually verified as the difference in the horizontal positions of the curves. If the antibiotic activity of the isomer were the same as that of tylosin, the two curves would be in exactly the same position. (3) If a right-shift of the position of the curve is statistically significant, then the antibiotic activity of the isomer is lower than that of tylosin. The errors on the EC_{50} values for pre- and post-photolysis solutions do not overlap, demonstrating a statistically significant decrease in antibiotic activity for the latter solution. It was concluded, therefore, that the isomer has less antibiotic activity than tylosin based on the shift observed in **Figure 3**.

Using the parameters and standard error values gained from the fitting of eq 1 to the data in **Figure 3**, tylosin was calculated to have an EC_{50} of 145 ± 13 μM. The proposed photoisomer γ/δ-*cis*-tylosin has an antibiotic activity lower than that of tylosin. From the observed shift in aggregate EC_{50} of the two compounds in the postphotolysis solution, and assuming a 1:1 interconversion between tylosin and the isomer, the antibiotic activity of the isomer was calculated to be 0.26 ± 0.21 tylosin activity units. This results in a theoretical EC_{50} of $(1.6 \pm 1.3) \times 10^3$ μM for the isomer, assuming the slope factor is similar. The error reported for this value was propagated from the EC_{50} values of the control and photoisomerized tylosin stock solutions, which were obtained from the asymptotic standard errors in the parameters for curve-fitting as described in the Materials and Methods section.

Environmental Photochemistry. The application of quantum yield values and absorbance data to the modeling of environmental photodegradation is described in detail by Leifer (*14*) and Schwarzenbach et al. (*15*). The wavelength-dependent rates of photon absorption for a compound are important data, calculated from its molar absorptivity spectrum and the average photon flux seen by the compound as a function of wavelength. One reason that wavelength-dependence is important to consider is that natural water bodies have different wavelength-dependent light attenuation characteristics. This raises a complication in the photolysis of tylosin because the absorption spectra of tylosin and the photoisomer are different, and therefore the resultant distribution of the photoisomers will theoretically be wavelength-dependent. The light attenuation in the water column due to natural organic matter increases exponentially at shorter wavelengths, and the fraction [tylosin]/([tylosin] + [isomer]) may theoretically be expected to increase slightly with depth.

Fortunately, this selection by light-screening for one tylosin photoisomer over the other is not expected to be significant in environmental systems. In photolysis experiments using varying SRFA concentrations in this study, no change in the equilibrium value for photoisomerization was observed, despite a large light screening effect (light screening factor $S = 0.6$ with 20 mg L^{-1} SRFA; see Supporting Information for calculation of S). Additional calculations verify that in a practical sense, natural light attenuation is not expected to significantly affect the isomer ratio in most natural systems. For example, consider a body of water with a 1 m photic zone and typical spectral shape parameters for a dark water body, $\alpha_g(412) = 3\ m^{-1}$ (attenuation at the reference wavelength $\lambda_{ref} = 412$ nm) and $s_e = 0.015\ nm^{-1}$ (spectral slope coefficient) for the common model for light absorption by dissolved organic matter shown in eq 4 (*20*).

$$\alpha_g(\lambda) = \alpha_g(\lambda_{ref}) \exp[-s_e(\lambda - \lambda_{ref})] \quad (4)$$

The resultant integrated action spectra for tylosin and the photoisomer averaged over the photic zone were calculated to decrease to 13% and 14% of their original magnitudes, respectively. This results in a change in the equilibrium value of [tylosin]/([tylosin] + [isomer]) from 0.50 to 0.51. Thus, even in the case of strong, selective light attenuation, the change in isomer distribution is not significant. Prediction of photochemical loss can therefore be made using the postequilibration average molar absorptivity spectrum for the tylosin/isomer mixture (tabulated in the Supporting Information) and the reported average quantum yield for photolysis, $(1.4 \pm 0.3) \times 10^{-3}$.

A similar calculation can be performed to account for the difference in light spectra when changing systems from the solar simulator used in this study to natural sunlight. For this calculation we used the incident radiation spectrum of the solar simulator and the spectrum of sunlight modeled using the SMARTS software package (*21*, *22*), as well as the quantum yields and decadic molar absorptivity spectra from this study. The fraction [tylosin]/([tylosin] + [isomer]) rises from 0.50 in the solar simulator to 0.53 under natural sunlight. Compared to the error in the direct photolysis quantum yield, this difference in the isomer distribution is negligible.

The rapid photoisomerization of tylosin is a novel phenomenon among antibiotics under high-volume use as growth promoters. No other macrolide antibiotic contains the chromophoric ketodiene functionality of tylosin. It is unique among the macrolides for both its absorption of light within the solar spectrum, as well as the rapid, efficient cis/trans photoisomerization.

ACKNOWLEDGMENT

The authors thank the National Research Initiative of the USDA Cooperative State Research, Education and Extension Service (Grant Number 2003-35107-13830) for financial support of this work and the Mentor Connection program and Hopkins High School for providing M.C. the opportunity to participate in this research. The assistance of K. Brook Jacobson and Jenna M. Schroeder in conducting the antibiotic activity assays is greatly appreciated.

Supporting Information Available: Further description of photochemical experiments and calculations performed, spectra of solar simulator and natural sunlight, HPLC chromatogram of tylosin and photoisomer, kinetic data for concentration-dependent and pH-dependent photolysis, kinetic data for photolysis with varied SRFA concentration, MS data for pre- and postirradiation samples, ^{1}H NMR data for pre- and postirradiation samples, concentration-corrected plot of the data in **Figure 1** including a fit to eq 3, and a tabulated list of UV−vis absorbance data for tylosin, the tylosin/isomer mixture and the calculated spectrum for the isomer. This material is available free of charge via the Internet at http://pubs.acs.org.

LITERATURE CITED

(1) Aarestrup, F. M.; Carstensen, B. Effect of tylosin used as a growth promoter on the occurrence of macrolide-resistant *Enterococci* and *Staphylococci* in pigs. *Microb. Drug Resist.* **1998**, *4*, 307−312.

(2) Onan, L. J.; LaPara, T. M. Tylosin-resistant bacteria cultivated from agricultural soil. *FEMS Microbiol. Lett.* **2003**, *220*, 15−20.

(3) Kolpin, D. W.; Furlong, E. T.; Meyer, M. T.; Thurman, E. M.; Zaugg, S. D.; Barber, L. B.; Buxton, H. T. Pharmaceuticals, hormones and other organic wastewater contaminants in U.S. streams, 1999−2000: a national reconnaissance. *Environ. Sci. Technol.* **2002**, *36*, 1202−1211.

(4) Halling-Sørensen, B.; Jacobsen, A.-M.; Jensen, J.; Sengeløv, G.; Vaclavik, E.; Ingerslev, F. Dissipation and effects of chlortetracycline and tylosin in two agricultural soils: a field-scale study in southern Denmark. *Environ. Toxicol. Chem.* **2005**, *24*, 802−810.

(5) Loke, M.-L.; Ingerslev, F.; Halling-Sørensen, B.; Tjørnelund, J. Stability of tylosin A in manure containing test systems determined by high performance liquid chromatography. *Chemosphere* **2000**, *40*, 759−765.

(6) Ingerslev, F.; Toräng, L.; Loke, M.-L.; Halling-Sørensen, B.; Nyholm, N. Primary biodegradation of veterinary antibiotics in aerobic and anaerobic surface water simulation systems. *Chemosphere* **2001**, *44*, 865−872.

(7) Paesen, J.; Cypers, W.; Pauwels, K.; Roets, E.; Hoogmartens, J. Study of the stability of tylosin A in aqueous solutions. *J. Pharm. Biomed. Anal.* **1995**, *13*, 1153−1159.

(8) Loke, M.-L.; Tjørnelund, J.; Halling-Sørensen, B. Determination of the distribution coefficient (log K_d) of oxytetracycline, tylosin A, olaquindox, and metronidazole in manure. *Chemosphere* **2002**, *48*, 351−361.

(9) Halling-Sørensen, B.; Sengeløv, G.; Ingerslev, F.; Jensen, L. B. Reduced antimicrobial potencies of oxytetracycline, tylosin, sulfadiazin, streptomycin, ciprofloxacin, and olaquindox due to environmental processes. *Arch. Environ. Contam. Toxicol.* **2003**, *44*, 7−16.

(10) Paesen, J.; Cypers, W.; Busson, R.; Roets, E.; Hoogmartens, J. Isolation of decomposition products of tylosin using liquid chromatography. *J. Chromatogr., A* **1995**, *699*, 99−106.

(11) Hu, D.; Coats, J. R. Aerobic degradation and photolysis of tylosin in water and soil. *Environ. Toxicol. Chem.* **2007**, *26*, 884−889.

(12) Dulin, D.; Mill, T. Development and evaluation of sunlight actinometers. *Environ. Sci. Technol.* **1982**, *16*, 815−820.

(13) Zepp, R. G. Quantum yields for reaction of pollutants in dilute aqueous solution. *Environ. Sci. Technol.* **1978**, *12*, 327−329.

(14) Leifer, A. *The Kinetics of Environmental Aquatic Photochemistry: Theory and Practice*; American Chemical Society: Washington DC, 1988.

(15) Schwarzenbach, R. P.; Gschwend, P. M.; Imboden, D. M. *Environmental Organic Chemistry*, 2nd ed.; John Wiley & Sons, Inc.: Hoboken, NJ, 2003.

(16) Wammer, K. H.; LaPara, T. M.; McNeill, K.; Arnold, W. A.; Swackhamer, D. L. Changes in antibacterial activity of triclosan and sulfa drugs due to photochemical transformations. *Environ. Toxicol. Chem.* **2006**, *25*, 1480−1486.

(17) Simova, S.; Ivanova, G. Proton and carbon chemical shift assignment and solution-state conformation of the macrocyclic ring in the macrolide antibiotic tylosin in aprotic solvents. *Magn. Reson. Chem.* **1996**, *34*, 255−260.

(18) Edhlund, B. L.; Arnold, W. A.; McNeill, K. Aquatic photochemistry of nitrofuran antibiotics. *Environ. Sci. Technol.* **2006**, *40*, 5422−5427.
(19) Ivanov, P. M. CONFLEX/MM3 search/minimization study of the conformations of the macrolide antibiotic tylosin. *J. Mol. Struct.* **2002**, *606*, 217−229.
(20) Twardowski, M. S.; Boss, E.; Sullivan, J. M.; Donaghay, P. L. Modeling the spectral shape of absorption by chromophoric dissolved organic matter. *Mar. Chem.* **2004**, *89*, 69−88.
(21) Gueymard, C. A. SMARTS, A simple model of the atmospheric radiative transfer of sunshine: algorithms and performance assessment. Technical Report No. FSEC-PF-270−95; Florida Solar Energy Center: Cocoa, FL, 1995.
(22) Gueymard, C. A. Parameterized transmittance model for direct beam and circumsolar spectral irradiance. *Sol. Energy* **2001**, *75*, 325−346.

Received for review January 12, 2007. Revised manuscript received June 14, 2007. Accepted June 15, 2007.

JF070101H